Department of Chemistry
University of Cambridge

Hierarchical equations of motion

Adam Přáda

Trinity College

First-year report
PhD in Chemistry

June 2019

Acknowledgements

First and foremost, I would like to thank Prof. Stuart Althorpe for his guidance and help in my work. I would also like to thank George Trenins and Raz Benson for many discussions, which have furthered my knowledge. I am very grateful to the rest of the Althorpe group for providing a pleasant and productive environment for my research. Furthermore, I would like to thank my family and my girlfriend for their unwavering support. I am also grateful to the EPSRC for providing funding for my work.

Abstract

Methods based on path integral molecular dynamics (PIMD) are a family of chemical dynamics techniques which are a common way of treating nuclear quantum effects in condensed phase. One of the approximations shared by all of these is the neglect of quantum coherence. This is usually a reasonable assumption, because the large number of interactions present in a solid or a liquid typically leads to quick decoherence. To better understand the role that this assumption may have, we decided to explore a method for exact quantum dynamics in a dissipative environment. Hierarchical equations of motion (HEOM) are a computational method that describes time evolution of a system quantum density matrix coupled to a bath of harmonic oscillators, which in the appropriate limits yields the exact results. In this work, quantum HEOM were implemented both in their high-temperature form, omitting Matsubara frequency terms present in the bath time autocorrelation function, as well as the full form, which results in a many-dimensional set of coupled differential equations. The behaviour of HEOM was studied at various limits, including the low-temperature breakdown, and the importance of the Matsubara terms has been demonstrated. Carrying out a Wigner transform of HEOM, one can obtain a position-momentum phase space analogue, which at the limit of high temperature gives completely classical HEOM. These were implemented and compared to the quantum version. In addition, the computational program was tested by reproducing the results of Sakurai and Tanimura on the Morse oscillator and preliminary work has been done on the OH potential of a hydrated oxonium ion. Drawing from this work, we propose future studies of the blue shift, which currently plagues PIMD-based dynamics methods in strongly anharmonic potentials, and of the role of an explicit bath and quantum coherence in condensed phase dynamics.

Contents

Chapter 1

Introduction

Advances of molecular dynamics have made it possible to explain many chemical and physical phenomena from first principles.[1] For many purposes, atomic nuclei can be treated classically, but over the past few decades the shortcomings of this approximation have become increasingly apparent resulting in the emergence of a new field of quantum chemical/nuclear dynamics.[2]

For quantum nuclear dynamics in condensed phase, where the coherence effects can be neglected, a range of path integral based methods have been developed. Using Feynman path integrals, one can obtain an isomorphism which maps the quantum system onto an extended classical system, called a ring polymer.[3] These polymers exactly represent quantum statistics, and classical dynamics is routinely used to sample thermal averages of static variables in a method called path integral molecular dynamics (PIMD).[1] However, all the dynamics present is considered to be a mathematical tool, rather than a representation of reality. To calculate dynamical variables, like time correlation functions, a range of PIMD-based methods have been proposed, including centroid molecular dynamics (CMD),[4,5] ring polymer molecular dynamics (RPMD),[6] linearised semi-classical initial value representation (LSC-IVR)[7] and related methods (PA-CMD, TRPMD, etc.).[2] All of these were originally *ad hoc* propositions that were shown to yield correct answers in various limits. In 2015 a new theory has been proposed, called the Matsubara dynamics, which gives a quantum Boltzmann conserving classical component of the exact quantum dynamics, neglecting only real-time quantum coherence. It was shown that all the previously mentioned methods are approximations to this more exact treatment.[8,9]

The most explicit way of accounting for the environment in condensed phase is by directly including the solvent molecules and converging the simulation with respect to the size of the box. This will naturally yield the most accurate results, but becomes impractical for larger systems or more computa-

tionally expensive methods.[10] An alternative is treating the surroundings as a non-specific bath, rather than explicit molecules, which is typically modelled as an ensemble of harmonic oscillators. We can push the abstraction even further and generalise the effect of the bath into new equations of motion only for the system of interest. Termed dissipative dynamics, for classical particles such treatment is described using the (generalised) Langevin equation or in case of probability distributions using the Fokker-Planck equation.[11,12] However, there is not a simple way of deriving equivalent quantum equations, which poses a severe limitation given the computational cost of quantum methods.

If the bath is considered to have an effectively infinite temperature, it is possible to use the stochastic Liouville equation[13] and this approach has seen many successes including the prediction of NMR and Mössbauer spectra and of dielectric relaxation.[14] However, in this treatment only fluctuations are present and no dissipation. This means that particles in a continuous coordinate, like a potential well, can never reach thermal equilibrium, which limits its applicability.[14] To overcome this drawback, Tanimura proposed a new approach called the hierarchical equations of motion (HEOM).[15] These were based on his previous work with Kubo[16,17] on stochastic and dynamic approaches to quantum decoherence and further developed in collaboration Wolynes.[18,19] HEOM can be used to derive equations of motion for a reduced density matrix of a system in a dissipative bath, which in appropriate limits are exact. These result in a theoretically infinite hierarchy of coupled differential equations in an infinite-dimensional space. However, as shown in the literature, this hierarchy can be effectively truncated to give a viable computational method.[14,18,19] HEOM were used to calculate a wide range of phenomena like vibrational spectra and electronic spectra, including multi-dimensional and non-linear spectroscopy,[20] reaction rates[21] and even energy transfer in light harvesting proteins.[22]

The aim of this work was to implement the hierarchical equations and to understand their behaviour under a range of conditions. This was to be carried out both in the high-temperature approximation, when Matsubara terms in the bath time autocorrelation function are neglected, as well as in the full low-temperature HEOM treatment, where a more complicated hierarchy of differential equations has to be solved. In addition, HEOM can be Wigner transformed into the position-momentum phase space, which at appropriate limits gives fully classical HEOM. The ability to calculate the exact behaviour of the dissipative system will be an invaluable tool in future studies of the shortcomings of the Matsubara-dynamics based methods including the role of a bath and of quantum coherence.

In the next chapter we recapitulate the background theory for quantum dissipative dynamics and guide the reader through the crucial steps of the HEOM derivation. In Chapter 3 we present the results of our computational implementation of the HEOM and discuss their importance. We conclude by summarising our findings and laying down propositions for future work in Chapter 4.

Chapter 2

Background theory

In this chapter we present the theoretical background, important derivations and approximative treatments required for this work. In section 2.1 a brief introduction to the description of quantum systems using density operators based on standard literature is given.[11,12,23–25] In section 2.2 the system-bath model used throughout this work is described. In sections 2.3–2.5 the reader is guided through the derivation of the hierarchical equations of motion using the Feynman-Vernon functional. The following section 2.6 explains how the infinite hierarchy can be truncated in a numerical simulation, and the last section 2.7 shows that using Wigner transforms we can obtain a classical analogue of the quantum equations of motion.

2.1 Density operators

2.1.1 Pure states

When systems are described in quantum physics, a typical object to use is a wave function $\psi(t)$, which satisfies Schrödinger's equation

$$\mathrm{i}\hbar\frac{\partial}{\partial t}|\psi\rangle = \hat{H}|\psi\rangle. \tag{2.1}$$

An alternative way of describing the system is using a density operator $\hat{\rho}$, which for a pure quantum state is defined as

$$\hat{\rho} \equiv |\psi\rangle\langle\psi|. \tag{2.2}$$

If we expand ψ in a basis set $\{\varphi_i\}$ as $\psi = \sum_n c_n\varphi_n$, then the density operator can be expressed as

$$\hat{\rho} = \sum_m \sum_n c_m c_n^* |\varphi_m\rangle\langle\varphi_n| \tag{2.3}$$

or as a matrix in the space of the basis vectors, which is how density operators are handled numerically,

$$\rho_{mn} = c_m c_n^*. \tag{2.4}$$

The diagonal elements then give the probabilities of finding the system in the particular state, resulting in the normalisation condition $\mathrm{Tr}[\hat{\rho}] = 1$, where Tr denotes the quantum mechanical trace. In addition, for any operator $\hat{A}$, the expectation value can be obtained as $\langle \hat{A} \rangle = \mathrm{Tr}[\hat{A}\hat{\rho}]$, which can be shown by expanding in any complete basis.

The equivalent of the Schrödinger's equation for density matrices is the quantum Liouville equation

$$\mathrm{i}\hbar \frac{\partial \hat{\rho}}{\partial t} = \hat{H}\hat{\rho} - \hat{\rho}\hat{H} = \hat{\mathcal{L}}\hat{\rho}, \tag{2.5}$$

where $\hat{\mathcal{L}}$ is the Liouvillian superoperator.

2.1.2 Statistical mixtures

In many physical situations we have ensembles of particles, where each particle can have many quantum states, but where the overall quantum state of the system is either not known or not of interest. Then, assuming that the individual particles have random complex phases relative to each other (i.e. the ensemble is not coherent), we can extend the definition of the density operator. If the probability of measuring quantum state ψ_j is P_j, then the density operator is

$$\hat{\rho} = \sum_j P_j |\psi_j\rangle\langle\psi_j|. \tag{2.6}$$

This is a very natural extension of the previous definition, because it preserves many of the properties of the pure state density operator. The diagonal elements still give the probability of finding the system in the specific state, but now also statistically averaged over the ensemble. The trace of a product with an operator $\langle \hat{A} \rangle = \mathrm{Tr}[\hat{A}\hat{\rho}]$ now gives the expectation value for the distribution. Importantly, the quantum Liouville equation (eq. 2.5) still holds.

2.2 System-bath model

Let us consider a model one-dimensional system coupled to a bath consisting of harmonic oscillators. The system is fully described by its mass m and potential $V_\mathrm{S}(\hat{q})$. The bath is described by the frequencies $\{\omega_j\}$, masses $\{m_j\}$ and coupling coefficients $\{c_j\}$ of the oscillators. The full Hamiltonian can then

be expressed as

$$\hat{H} = \frac{\hat{p}^2}{2m} + V_{\mathrm{S}}(\hat{q}) + \sum_j \left[\frac{\hat{p}_j^2}{2m_j} + \frac{m_j \omega_j^2}{2} \left(\hat{x}_j - \frac{c_j \hat{q}}{m_j \omega_j^2} \right)^2 \right], \tag{2.7}$$

where $\hat{p}$ and $\hat{q}$ describe the system, and $\{\hat{p}_j\}$ and $\{\hat{x}_j\}$ describe the bath. We can split the full Hamiltonian into three parts

$$\hat{H} = \hat{H}_{\mathrm{S}} + \hat{H}_{\mathrm{B}} + \hat{H}_{\mathrm{SB}}. \tag{2.8}$$

The system Hamiltonian is

$$\hat{H}_{\mathrm{S}} = \frac{\hat{p}^2}{2m} + V(\hat{q}), \tag{2.9}$$

where

$$V(\hat{q}) = V_{\mathrm{S}}(\hat{q}) + \frac{a_{\mathrm{ren}}}{2} \hat{q}^2 \tag{2.10}$$

with

$$a_{\mathrm{ren}} = \sum_j \frac{c_j^2}{m_j \omega_j^2}, \tag{2.11}$$

the bath Hamiltonian is

$$\hat{H}_{\mathrm{B}} = \sum_j \left[\frac{\hat{p}_j^2}{2m_j} + \frac{m_j \omega_j^2}{2} \hat{x}_j^2 \right] \tag{2.12}$$

and the interaction Hamiltonian is

$$\hat{H}_{\mathrm{SB}} = -\hat{X}(\hat{\boldsymbol{x}}) \hat{q}, \tag{2.13}$$

where $\hat{X}$ is the collective bath coordinate operator given by

$$\hat{X}(\hat{\boldsymbol{x}}) = \sum_j c_j \hat{x}_j, \tag{2.14}$$

where the vector $\hat{\boldsymbol{x}} = \{\hat{x}_j\}$. The reason for this form, which includes the renormalisation potential, is to maintain translational symmetry for $V_S(\hat{q}) = 0$.[26]

For a set of states $\{|q_i, \boldsymbol{x}_i\rangle\}$ in the Hilbert space of system and bath coordinates with probabilities $\{P_i\}$, the density operator is

$$\hat{\rho}(q, \boldsymbol{x}) = \sum_i P_i |q_i, \boldsymbol{x}_i\rangle\langle q_i, \boldsymbol{x}_i|, \tag{2.15}$$

where the quantities in parentheses denote the Hilbert space in which the

density operator is defined. A corresponding density matrix in the position representation would then be

$$\rho(q, \boldsymbol{x}; q', \boldsymbol{x}') = \langle q, \boldsymbol{x}|\hat{\rho}|q', \boldsymbol{x}'\rangle, \tag{2.16}$$

where the functions in parentheses denote the coordinate values at which the matrix element is calculated.

In the Schrödinger picture, which we shall adopt, the operators are constant in time, while the wave functions evolve. However, the density operator is an exception to this rule since it is an operator composed of wave functions. To denote this time dependence we shall use the notation

$$\hat{\rho}(q, \boldsymbol{x}; t = \tau) = \hat{\rho}_\tau(q, \boldsymbol{x}) \text{ and } \rho(q, \boldsymbol{x}; q', \boldsymbol{x}'; t = \tau) = \rho_\tau(q, \boldsymbol{x}; q', \boldsymbol{x}'). \tag{2.17}$$

2.3 Feynman-Vernon influence functional

We aim to obtain the equations of motion for the system. The state of the full system-bath set-up is described by a density operator $\hat{\rho}(q, \boldsymbol{x})$. At a non-zero time, the density operator can be expressed using the time propagation operators as

$$\hat{\rho}_t(q, \boldsymbol{x}) = \mathrm{e}^{-\mathrm{i}\hat{H}(q,\boldsymbol{x})t/\hbar}\hat{\rho}_0(q, \boldsymbol{x})\mathrm{e}^{+\mathrm{i}\hat{H}(q,\boldsymbol{x})t/\hbar}. \tag{2.18}$$

Given that we are interested only in the state of the system at time t, we can trace out the bath degrees of freedom to obtain a reduced density operator

$$\hat{\rho}_t(q) = \int \mathrm{d}\boldsymbol{x}\langle \boldsymbol{x}|\hat{\rho}_t(q, \boldsymbol{x})|\boldsymbol{x}\rangle, \tag{2.19}$$

where $\int \mathrm{d}\boldsymbol{x}$ denotes integration over all bath degrees of freedom.

In addition, we shall assume that the whole system was initially in a factorised state, i.e. $\hat{\rho}(q, \boldsymbol{x}) = \hat{\rho}(q)\hat{\rho}(\boldsymbol{x})$ and that the bath was in a thermal equilibrium ($\rho_0(\boldsymbol{x}, \boldsymbol{x}') = \langle \boldsymbol{x}|\mathrm{e}^{-\beta\hat{H}_B}/Z_\mathrm{B}|\boldsymbol{x}'\rangle$), but not in equilibrium with the system. This can be done without loss of generality, because we can account for initial correlations once we obtain the hierarchy of density operators.[15] We obtain

$$\rho_0(q, \boldsymbol{x}; q', \boldsymbol{x}') = \rho_0(q, q')\rho_0(\boldsymbol{x}, \boldsymbol{x}') = \rho_0(q, q')\langle \boldsymbol{x}|\frac{\mathrm{e}^{-\beta\hat{H}_B}}{Z_\mathrm{B}}|\boldsymbol{x}'\rangle \tag{2.20}$$

where the inverse temperature $\beta = 1/(k_\mathrm{B}T)$. With this initial matrix and using standard identities, the density matrix at time t can be cast into the

form[‡]

$$\rho_t(q_t, q_t') = \int \mathrm{d}q_0 \int \mathrm{d}q_0' \int \mathrm{d}\boldsymbol{x}_0 \int \mathrm{d}\boldsymbol{x}_0' \int \mathrm{d}\boldsymbol{x}\ \langle q_t, \boldsymbol{x}|\mathrm{e}^{-\mathrm{i}\hat{H}t/\hbar}|q_0, \boldsymbol{x}_0\rangle \times \rho_0(q_0, q_0')\langle \boldsymbol{x}_0|\frac{\mathrm{e}^{-\beta\hat{H}_B}}{Z_\mathrm{B}}|\boldsymbol{x}_0'\rangle\langle q_0', \boldsymbol{x}_0'|\mathrm{e}^{+\mathrm{i}\hat{H}t/\hbar}|q_t', \boldsymbol{x}\rangle \quad (2.21)$$

This integral can be re-written using the Feynman-Vernon influence functional as[27]

$$\rho_t(q_t, q_t') = \int \mathrm{d}q_0 \int \mathrm{d}q_0' \int_{q_0=q(0)}^{q_t=q(t)} \mathcal{D}[q(\tau)] \int_{q_0'=q'(0)}^{q_t'=q'(t)} \mathcal{D}[q'(\tau)]\ \rho_0(q_0, q_0') \times F_t(q(\tau), q'(\tau))G_t(q(\tau), q'(\tau)), \quad (2.22)$$

where $\int \mathcal{D}[q(\tau)]$ denotes a Feynman path integral,[3] G_t is the propagator/kernel for an isolated system and F_t is the influence functional. The propagator is given by

$$G_t(q(\tau), q'(\tau)) = \exp\left[\frac{\mathrm{i}}{\hbar}\big[S_\mathrm{S}(q(\tau); t) - S_\mathrm{S}(q'(\tau); t)\big]\right], \quad (2.23)$$

where the classical action for an isolated system is [†]

$$S_\mathrm{S}(q(\tau); t) = \int_0^t \mathrm{d}\tau\ L(\dot{q}, q, \tau) = \int_0^t \mathrm{d}\tau \left[\frac{m\dot{q}^2(\tau)}{2} - V\big(q(\tau)\big)\right], \quad (2.24)$$

with L denoting the Lagrangian. All system-bath interaction is contained in the influence functional which is given by

$$F_t(q(\tau), q'(\tau)) = \int \mathrm{d}\boldsymbol{x}_0 \int \mathrm{d}\boldsymbol{x}_0' \int \mathrm{d}\boldsymbol{x} \int \mathcal{D}[\boldsymbol{x}(t)] \int \mathcal{D}[\boldsymbol{x}'(t)]\ \rho_0(\boldsymbol{x}_0, \boldsymbol{x}_0') \times\exp\left[\frac{\mathrm{i}}{\hbar}[S_\mathrm{B}(\boldsymbol{x}(\tau); t) - S_\mathrm{B}(\boldsymbol{x}'(\tau); t) + S_\mathrm{SB}(q(\tau), \boldsymbol{x}(\tau); t) - S_\mathrm{SB}(q'(\tau), \boldsymbol{x}'(\tau); t)]\right], \quad (2.25)$$

where S_B and S_SB are the classical actions for the bath and for the interaction

[‡]The Feynman path integral notation requires position to be a function of time. This can be at first sight contradictory to the Schrödinger picture, in which the position operator is time independent. It can be reconciled by considering $q_\tau \equiv q(\tau)$ with $\tau \neq t$ as a dummy variable emerging from the identity $\hat{I} = \int \mathrm{d}q_\tau |q_\tau\rangle\langle q_\tau|$, while $q_t \equiv q$ is the position basis set in which the density matrix is represented.

[†]We have moved from the operator notation to the eigenvalues in the position basis, i.e. $\hat{q} \to q$ since these are the classical actions.

respectively and are given by

$$S_{\mathrm{B}}(\boldsymbol{x}(\tau);t)=\int_0^t \mathrm{d}\tau \sum_j \left[\frac{m_j\dot{x}_j^2(\tau)}{2}-\frac{m_j\omega_j^2}{2}x_j^2(\tau)\right] \tag{2.26}$$

and

$$S_{\mathrm{SB}}(q(\tau),\boldsymbol{x}(\tau);t)=\int_0^t \mathrm{d}\tau\big[+X(\boldsymbol{x}(\tau))q(\tau)\big]. \tag{2.27}$$

The functional integration in eq. 2.25 can be done exactly for this system and yields[26]

$$F_t(q(\tau),q'(\tau))=\exp\Bigg[-\frac{1}{\hbar^2}\int_0^t \mathrm{d}\tau' \int_0^{\tau'} \mathrm{d}\tau[q(\tau')-q'(\tau')] \times [\alpha(\tau'-\tau)q(\tau)-\alpha^*(\tau'-\tau)q'(\tau)]\Bigg], \tag{2.28}$$

where $\alpha(t)=\langle\hat{X}(\tau)\hat{X}(\tau+t)\rangle$ is the time autocorrelation function of the collective bath coordinate given by

$$\alpha(t)=\hbar\sum_j \frac{c_j^2}{2m_j\omega_j}\left(\mathrm{e}^{-\mathrm{i}\omega_j t}+\frac{\mathrm{e}^{+\mathrm{i}\omega_j t}+\mathrm{e}^{-\mathrm{i}\omega_j t}}{\mathrm{e}^{\beta\hbar\omega_j}-1}\right). \tag{2.29}$$

Following the convention in the literature, we can define

$$q^{\circ}(t)\equiv q(t)+q'(t) \text{ and } q^{\times}(t)\equiv q(t)-q'(t), \tag{2.30}$$

which in operator notation is equivalent to the commutator and anti-commutator superoperators

$$\hat{A}^{\circ}\hat{B}\equiv\hat{A}\hat{B}+\hat{B}\hat{A}=[\hat{A},\hat{B}]_+ \text{ and } \hat{A}^{\times}\hat{B}\equiv\hat{A}\hat{B}-\hat{B}\hat{A}=[\hat{A},\hat{B}]. \tag{2.31}$$

This simplifies the formula for the influence functional to

$$F_t(q(\tau),q'(\tau))=\exp\Bigg[-\frac{1}{\hbar^2} \times\int_0^t \mathrm{d}\tau' q^{\times}(\tau')\int_0^{\tau'} \mathrm{d}\tau[\alpha(\tau'-\tau)q(\tau)-\alpha^*(\tau'-\tau)q'(\tau)]\Bigg]. \tag{2.32}$$

Considering the real and imaginary parts of $\alpha(t)$

$$\alpha_{\mathrm{R}}(t)=\hbar\sum_j \frac{c_j^2}{2m_j\omega_j}\cos(\omega_j t)\coth\left(\frac{\beta\hbar\omega_j}{2}\right), \tag{2.33}$$

$$\alpha_{\rm I}(t) = -\hbar \sum_j \frac{c_j^2}{2m_j\omega_j} \sin(\omega_j t), \tag{2.34}$$

where

$$\alpha_{\rm R} \equiv {\rm Re}\{\alpha\},\ \alpha_{\rm I} \equiv {\rm Im}\{\alpha\}, \tag{2.35}$$

we can further simplify the influence functional to

$$F_t(q(\tau), q'(\tau)) = \\ \exp\left[-\frac{1}{\hbar^2}\int_0^t {\rm d}\tau'\ q^\times(\tau') \int_0^{\tau'} {\rm d}\tau \Big(\alpha_{\rm R}(\tau'-\tau)q^\times(\tau) + {\rm i}\alpha_{\rm I}(\tau'-\tau)q^\circ(\tau)\Big)\right] \tag{2.36}$$

The functional integrals in eq. 2.22 can be rewritten as infinite sums and products in discretised time following Feynman's definition[3] to give

$$\rho_t(q_t, q_t') = \int' {\rm d}\boldsymbol{q} \int' {\rm d}\boldsymbol{q}'\ \rho_0(q_0, q_0') F_t(\boldsymbol{q}, \boldsymbol{q}') G_t(\boldsymbol{q}, \boldsymbol{q}'), \tag{2.37}$$

where $\boldsymbol{q} = \{q_0, \ldots, q_n, \ldots, q_N\}$, with $q_N \equiv q_t$. The integrals are $\int' {\rm d}\boldsymbol{q} = \int {\rm d}q_0\ \cdots \int {\rm d}q_n \cdots \int {\rm d}q_{N-1}$, i.e. integrals over all q_n's except for q_t. In this notation the influence functional is given by

$$F_t(\boldsymbol{q}, \boldsymbol{q}') = \exp\left[-\frac{\epsilon^2}{\hbar^2}\sum_{n=0}^{N} w_n q_n^\times \sum_{m=0}^{n} w_m \Big(\alpha_{\rm R}(t_n - t_m)q_m^\times + {\rm i}\alpha_{\rm I}(t_n - t_m)q_m^\circ\Big)\right], \tag{2.38}$$

where $t_n = nt/N$, $\epsilon = t/N$ and

$$w_n = \begin{cases} 1/2 & \text{for } n = 0, N \\ 1 & \text{otherwise} \end{cases}, \tag{2.39}$$

and $G_t(\boldsymbol{q}, \boldsymbol{q}')$ is given by[†]

$$G_t(\boldsymbol{q}, \boldsymbol{q}') = \langle q_N|{\rm e}^{-{\rm i}\hat{H}_{\rm S}\epsilon/\hbar}|q_{N-1}\rangle\langle q_{N-1}|{\rm e}^{-{\rm i}\hat{H}_{\rm S}\epsilon/\hbar}|q_{N-2}\rangle \ldots \langle q_1|{\rm e}^{-{\rm i}\hat{H}_{\rm S}\epsilon/\hbar}|q_0\rangle \\ \times \langle q_N'|{\rm e}^{+{\rm i}\hat{H}_{\rm S}\epsilon/\hbar}|q_{N-1}'\rangle\langle q_{N-1}'|{\rm e}^{+{\rm i}\hat{H}_{\rm S}\epsilon/\hbar}|q_{N-2}'\rangle \ldots \langle q_1'|{\rm e}^{+{\rm i}\hat{H}_{\rm S}\epsilon/\hbar}|q_0'\rangle. \tag{2.40}$$

[†]By using Trotter factorisation, splitting $\exp(-{\rm i}\hat{H}/\hbar)$ into the kinetic and potential part, inserting position representation identities $\hat{I} = \int {\rm d}q_\tau |q_\tau\rangle\langle q_\tau|$ and evaluating the kinetic energy operator in position representation as $\langle q_1|\exp(-{\rm i}\epsilon\hat{T}/\hbar)|q_2\rangle = \sqrt{2\pi\hbar m/(\epsilon{\rm i})}\exp({\rm i}m(q_2 - q_1)^2/(2\hbar\epsilon))$, we can show that $\int_{q_0}^{q} \mathcal{D}q(\tau)\exp(\frac{\rm i}{\hbar}S(q(\tau), t)) = \langle q_0|\exp(-{\rm i}\hat{H}/\hbar)|q_t\rangle$.

2.4 Bath description

Given the form of the equations presented in the previous section, the whole harmonic oscillator bath can be represented using a single function $J(\omega)$, typically termed the spectral density, which we shall define as

$$J(\omega) = \hbar \sum_j \frac{c_j^2}{2m_j\omega_j}\delta(\omega - \omega_j). \tag{2.41}$$

This simplifies the equations for α's to

$$\alpha(t) = \int_0^\infty \mathrm{d}\omega\ J(\omega)\left(\mathrm{e}^{-\mathrm{i}\omega t} + \frac{\mathrm{e}^{+\mathrm{i}\omega t} + \mathrm{e}^{-\mathrm{i}\omega t}}{\mathrm{e}^{\beta\hbar\omega} - 1}\right), \tag{2.42}$$

$$\alpha_\mathrm{R}(t) = \int_0^\infty \mathrm{d}\omega\ J(\omega)\cos(\omega t)\coth\left(\frac{\beta\hbar\omega}{2}\right), \tag{2.43}$$

and

$$\alpha_\mathrm{I}(t) = -\int_0^\infty \mathrm{d}\omega\ J(\omega)\sin(\omega t), \tag{2.44}$$

as well as the expression for a_ren

$$a_\mathrm{ren} = 2\int_0^\infty \mathrm{d}\omega\ \frac{J(\omega)}{\hbar\omega}. \tag{2.45}$$

Negative frequencies of harmonic oscillators in the bath are not physical, but if we define $J(\omega)$ to be an odd function, i.e. $J(\omega) = -J(-\omega)$,[‡] we can express α's also as

$$\alpha(t) = \int_{-\infty}^\infty \mathrm{d}\omega\ J(\omega)\frac{\mathrm{e}^{+\mathrm{i}\omega t}}{\mathrm{e}^{\beta\hbar\omega} - 1}, \tag{2.46}$$

$$\alpha_\mathrm{R}(t) = \frac{1}{2}\int_{-\infty}^\infty \mathrm{d}\omega\ J(\omega)\cos(\omega t)\coth\left(\frac{\beta\hbar\omega}{2}\right) \tag{2.47}$$

and

$$\alpha_\mathrm{I}(t) = -\frac{1}{2}\int_{-\infty}^\infty \mathrm{d}\omega\ J(\omega)\sin(\omega t), \tag{2.48}$$

which, as we shall see, may be easier to evaluate.

Following the literature[16,26,28,29], we have chosen the Debye bath (also Drude bath or Ohmic bath with Lorentz-Drude cutoff), the spectral density of which takes the form

$$J(\omega) = \frac{\hbar\eta}{\pi}\frac{\gamma^2\omega}{\gamma^2 + \omega^2}, \tag{2.49}$$

where η is the strength of the bath coupling and γ is the cutoff frequency.

[‡]This is equivalent to redefining $J \equiv \hbar\sum_j \frac{c_j^2}{2m_j\omega_j}[\delta(\omega - \omega_j) - \delta(\omega + \omega_j)]$. Note that this does not retain the normalisation of J, but doubles it.

The form of α is then

$$\alpha(t) = \frac{\hbar\eta\gamma^2}{\pi}\int_{-\infty}^{\infty} \mathrm{d}\omega\ \frac{\omega}{\gamma^2+\omega^2}\frac{\mathrm{e}^{+\mathrm{i}\omega t}}{\mathrm{e}^{\beta\hbar\omega}-1}, \tag{2.50}$$

which can be evaluated by contour integration in the complex plane along contours $z_1 = R,\ R \in (-\infty, \infty)$ and $z_2 = \lim_{R\to\infty} R\mathrm{e}^{-\mathrm{i}\theta},\ \theta \in [0, \pi]$. This contour contains poles at $z = -\mathrm{i}\gamma$ and at $z = -\mathrm{i}\gamma_k$ where $\gamma_k = 2\pi k/(\beta\hbar),\ k = 1, 2, 3, \ldots$ are the Matsubara frequencies. This yields

$$\alpha(t) = \sum_{k=0}^{\infty} C_k \mathrm{e}^{-\gamma_k t}, \tag{2.51}$$

where $\gamma_0 \equiv \gamma$ and where the coefficients are given by

$$\begin{aligned} C_0 &= \frac{\hbar\eta\gamma^2}{2}\left[\cot\left(\frac{\beta\hbar\gamma}{2}\right) - \mathrm{i}\right], \\ C_{k>0} &= \frac{2\eta\gamma^2}{\beta}\frac{\gamma_k}{\gamma_k^2-\gamma^2}. \end{aligned} \tag{2.52}$$

In the rest of this work we shall refer to the $k > 0$ terms as the Matsubara terms because of the appearance of Matsubara frequencies $\gamma_{k>0}$. The formulae for the real and imaginary parts are then

$$\alpha_{\mathrm{R}}(t) = \frac{\hbar\eta\gamma^2}{2}\cot\left(\frac{\beta\hbar\gamma}{2}\right)\mathrm{e}^{-\gamma t} + \sum_{k=1}^{\infty} C_k \mathrm{e}^{-\gamma_k t} \tag{2.53}$$

and

$$\alpha_{\mathrm{I}}(t) = -\frac{\hbar\eta\gamma^2}{2}\mathrm{e}^{-\gamma t}. \tag{2.54}$$

For the renormalisation coefficient in eq. 2.45 the chosen spectral density gives

$$a_{\mathrm{ren}} = \eta\gamma. \tag{2.55}$$

2.5 Hierarchical equations of motion (HEOM)

To obtain the equations of motion for the density matrix, we differentiate it with respect to time. This is most easily done with the continuous form of equations (eq. 2.22 for ρ and eq. 2.32 for F_t). Firstly we shall assume the general form of α given by eq. 2.51. Carefully differentiating and observing the emerging patterns, one can obtain an infinite network of coupled differential equations for a hierarchy of density matrices[30,31]

$$\begin{aligned}
\frac{\partial \hat{\rho}_{\{0\}}}{\partial t} &= -\frac{\mathrm{i}}{\hbar}\hat{\mathcal{L}}\hat{\rho}_{\{0\}} - \frac{\mathrm{i}}{\hbar}\hat{q}^{\times}\sum_{k=0}^{\infty}\hat{\rho}_{\{0\}_k^+} \\
&\cdots \\
\frac{\partial \hat{\rho}_{\boldsymbol{n}}}{\partial t} &= -\left(\frac{\mathrm{i}}{\hbar}\hat{\mathcal{L}} + \sum_{k=0}^{\infty} n_k\gamma_k\right)\hat{\rho}_{\boldsymbol{n}} - \frac{\mathrm{i}}{\hbar}\hat{q}^{\times}\sum_{k=0}^{\infty}\hat{\rho}_{\boldsymbol{n}_k^{\oplus}} - \frac{\mathrm{i}}{\hbar}\sum_{k=0}^{\infty} n_k\left(C_k\hat{q}\hat{\rho}_{\boldsymbol{n}_k^{\ominus}} - C_k^{*}\hat{\rho}_{\boldsymbol{n}_k^{\ominus}}\hat{q}\right) \\
&\cdots
\end{aligned} \tag{2.56}$$

where the Liouvillian is given by

$$\begin{gathered}
\hat{\mathcal{L}}\hat{\rho} = \hat{H}_{\mathrm{S}}^{\times}\hat{\rho} = \hat{H}_{\mathrm{S}}\hat{\rho} - \hat{\rho}\hat{H}_{\mathrm{S}} \\
\text{or} \\
\mathcal{L}(q,q') = H_{\mathrm{S}}(q) - H_{\mathrm{S}}(q')
\end{gathered} \tag{2.57}$$

and where $\hat{\rho}_{\boldsymbol{n}}$ are the auxiliary density operators (ADOs). These density operators are indexed by infinite-dimensional vectors $\boldsymbol{n} = \{n_k\},\ k = 0, 1, 2, \ldots$ Each component of these vectors can take all non-negative integer values $n_k = 0, 1, 2, \ldots$ We have also introduced the notation $\boldsymbol{n}_k^{\oplus/\ominus} = \{n_0, \ldots, n_{k-1}, n_k \pm 1, n_{k+1}, \ldots\}$. The $\hat{\rho}_{\boldsymbol{n}}$ with zero vector $\boldsymbol{n} = \{0\} = \{n_k\},\ n_k = 0\ \forall k$ is the physical density matrix $\hat{\rho}_t \equiv \hat{\rho}_{\{0\}}$ while all the ADOs are just an algebraically convenient way of handling these complex equations of motion, but bear no direct physical significance. It is also useful to define the tier of an ADO as

$$n = \sum_{k=0}^{\infty} n_k. \tag{2.58}$$

The ADOs are given by

$$\rho_{\boldsymbol{n}}(q,q') = \int \mathrm{d}q_0 \int \mathrm{d}q_0' \int_{q_0=q(0)}^{q_t=q(t)} \mathcal{D}[q(\tau)] \int_{q_0'=q'(0)}^{q_t'=q'(t)} \mathcal{D}[q'(\tau)]\ \rho_0(q_0,q_0') \\ \times F_t(q(\tau),q'(\tau)) G_t(q(\tau),q'(\tau)) \prod_{k=0}^{\infty} \left[\left(-\frac{\mathrm{i}}{\hbar} \right)^{n_k} f_k^{n_k}(q(\tau),q'(\tau),t) \right], \quad (2.59)$$

with

$$f_k(q(\tau),q'(\tau),t) = \int_0^t \mathrm{d}\tau \mathrm{e}^{-\gamma_k(t-\tau)} [C_k q(\tau) - C_k^* q'(\tau)], \quad (2.60)$$

which applies to $\rho_{\{0\}}(q,q')$ as well, hence the name auxiliary *density operator*.

Knowing the form of the coefficients C_k for the chosen bath, we can simplify the equations of motion using the fact that only C_0 has a non-zero imaginary part to obtain

$$\frac{\partial \hat{\rho}_{\boldsymbol{n}}}{\partial t} = -\left(\frac{\mathrm{i}}{\hbar}\hat{\mathcal{L}} + \sum_{k=0}^{\infty} n_k \gamma_k \right) \hat{\rho}_{\boldsymbol{n}} - \frac{\mathrm{i}}{\hbar} \hat{q}^{\times} \sum_{k=0}^{\infty} \hat{\rho}_{\boldsymbol{n}_k^{\oplus}} \\ - \frac{\mathrm{i}}{\hbar} (\mathrm{i} n_0 C_0^{\mathrm{I}}) \hat{q}^{\circ} \hat{\rho}_{\boldsymbol{n}_0^{\ominus}} - \frac{\mathrm{i}}{\hbar} \sum_{k=0}^{\infty} n_k C_k^{\mathrm{R}} \hat{q}^{\times} \hat{\rho}_{\boldsymbol{n}_k^{\ominus}}, \quad (2.61)$$

with $C_k^{\mathrm{R}} = \mathrm{Re}\{C_k\}$, which affects only C_0, and $C_0^{\mathrm{I}} \equiv \mathrm{Im}\{C_0\}$.

2.6 Truncating the infinite hierarchy

So far, all the equations were numerically exact within the given approximations. However, it is of course impossible to simulate an infinite hierarchy on a computer. Therefore, a truncation scheme is necessary. Following notation of Shi and Chen[21,32], we shall introduce two parameters: K and L.

K is the maximum index included in the exponential series of the time autocorrelation function α, turning eq. 2.51 into

$$\alpha(t) = \sum_{k=0}^{K} C_k \mathrm{e}^{-\gamma_k t}, \quad (2.62)$$

which propagates to all summations and products indexed by k in all definitions and the equations of motion.

L is the maximum tier (defined by eq. 2.58) present among the ADOs in the hierarchy.

Before we look into the truncation in both of these parameters, it is useful to consider a scaling scheme.

2.6.1 Scaling

Shi and Chen[21,32] proposed scaling ADOs as

$$\tilde{\rho}_{\boldsymbol{n}} = \left(\prod_{k=0}^{\infty} n_k! |C_k|^{n_k} \right)^{-1/2} \rho_{\boldsymbol{n}}, \tag{2.63}$$

which gives rise to equations of motion

$$\begin{aligned} \frac{\partial \hat{\rho}_{\boldsymbol{n}}}{\partial t} = &- \left(\frac{\mathrm{i}}{\hbar} \hat{\mathcal{L}} + \sum_{k=0}^{\infty} n_k \gamma_k \right) \hat{\rho}_{\boldsymbol{n}} - \frac{\mathrm{i}}{\hbar} \hat{q}^{\times} \sum_{k=0}^{\infty} \sqrt{(n_k+1)|C_k|} \hat{\rho}_{\boldsymbol{n}_k^{\oplus}} \\ &- \frac{\mathrm{i}}{\hbar} \sum_{k=0}^{\infty} \sqrt{n_k/|C_k|} \left(C_k \hat{q} \hat{\rho}_{\boldsymbol{n}_k^{\ominus}} - C_k^* \hat{\rho}_{\boldsymbol{n}_k^{\ominus}} \hat{q} \right). \end{aligned} \tag{2.64}$$

The scaling does not affect the physical density matrix or its dynamics. It also ensures that for large n the amplitude of ADOs tends to zero.

2.6.2 K: Truncating Matsubara terms

High temperature approximation

At high temperatures, the Matsubara frequencies $\gamma_k = 2\pi k/(\beta\hbar)$ grow sufficiently to effectively truncate the series of the bath time autocorrelation function α (eq. 2.51) at $k = 0$. This is equivalent to saying $\lim_{\beta \to 0} \exp(-\gamma_k t) = 0$ for $k \neq 0$. This simplifies eq. 2.61 to

$$\begin{aligned} \frac{\partial \hat{\rho}_n}{\partial t} = &- \left(\frac{\mathrm{i}}{\hbar} \hat{\mathcal{L}} + n\gamma \right) \hat{\rho}_n - \frac{\mathrm{i}}{\hbar} \hat{q}^{\times} \hat{\rho}_{n+1} \\ &- \frac{n_0 \eta \gamma^2}{2} \hat{q}^{\circ} \hat{\rho}_{n-1} - \frac{\mathrm{i}}{\hbar} \frac{n\hbar\eta\gamma^2}{2} \cot\left(\frac{\beta\hbar\gamma}{2} \right) \hat{q}^{\times} \hat{\rho}_{n-1}, \end{aligned} \tag{2.65}$$

where ADOs are no longer indexed by a K-dimensional vector $\boldsymbol{n}$, but only by its first component n_0, which is now equivalent to the tier of the ADO n (eq. 2.58). Thus the space of ADOs was "flattened" into one dimension, where each ADO depends only on the ADO above and below in the hierarchy.

Simple truncation

Terms up to $k = K$ are included explicitly and all terms with $k > K$ are discarded with no additional correction being made.

Ishizaki-Tanimura scheme

Ishizaki and Tanimura have suggested a Markovian treatment of the non-explicit k-terms.[14,30,33] This leads to new terms in the equations of motion (eq. 2.56), giving

$$\frac{\partial \hat{\rho}_{\boldsymbol{n}}}{\partial t} = -\left(\frac{\mathrm{i}}{\hbar}\hat{\mathcal{L}} + \sum_{k=0}^{K} n_k \gamma_k + \hat{\Xi}\right)\hat{\rho}_{\boldsymbol{n}} - \frac{\mathrm{i}}{\hbar}\hat{q}^{\times}\sum_{k=0}^{K}\hat{\rho}_{\boldsymbol{n}_k^{\oplus}} - \frac{\mathrm{i}}{\hbar}\sum_{k=0}^{K} n_k \left(C_k \hat{q}\hat{\rho}_{\boldsymbol{n}_k^{\ominus}} - C_k^{*}\hat{\rho}_{\boldsymbol{n}_k^{\ominus}}\hat{q}\right), \quad (2.66)$$

where the low T correction term $\hat{\Xi}$ is given by

$$\hat{\Xi} = \left(+\frac{\eta}{\beta\hbar^2} - \frac{1}{\hbar^2}\sum_{k=0}^{K}\frac{C_k^{\mathrm{R}}}{\gamma_k}\right)\hat{q}^{\times}\hat{q}^{\times} \quad (2.67)$$

This approximation should be justified as long as $\gamma_K \gg \Omega_0$, where Ω_0 is the characteristic frequency of the system.[30]

2.6.3 L: Truncating ADO level

Simple truncation

In this scheme, the ADOs are set to zero for tier $n > L$ (where n is given by eq. 2.58). One can simply converge the calculation with respect to L. However, if ADOs are scaled according to Shi and Chen as shown in section 2.6.1, then termination can be justified by a negligible magnitude of the discarded ADO. This can be implemented in the simulation as a pruning step, where at regular intervals all ADOs below the threshold are discarded.

Anchor equation

The second method, initially proposed by Tanimura,[18,30] uses an anchoring equation. Tanimura shows that for large enough tier n, ADOs can be approximated by an expression independent of $n+1$'st ADOs. However, when employed in calculations, scaling and simple truncation was found to be a more robust way of truncating L.

2.6.4 Initial state

Since we assumed the initial state to be of the factorised form (eq. 2.20), functions $f_k(q(\tau), q'(\tau), t = 0) = 0$ and only the physical density operator contributes at zero time, giving

$$\rho_{\{0\}}(q, q'; t = 0) = \rho_0(q, q'), \tag{2.68}$$

$$\rho_{\boldsymbol{n}}(q, q'; t = 0) = 0, \ \boldsymbol{n} \neq \{0\}. \tag{2.69}$$

This means that we do not have to evaluate f_k's explicitly since all ADOs emerge naturally during time evolution of the physical density matrix using HEOM. As Tanimura has shown, if a correlated initial state is required, it can be achieved by having non-zero ADOs at $t = 0$.[14,34]

2.7 HEOM in phase space

The classical analogues of density matrices are distribution functions. One way of representing quantum density matrices in classical phase space is using the Wigner transform.[35–37] A Wigner function $W(q, p)$ corresponding to a density operator $\hat{\rho}$ is given by

$$W(q, p) = \frac{1}{2\pi\hbar} \int_{-\infty}^{\infty} \mathrm{d}y \langle q - y/2|\hat{\rho}|q + y/2\rangle \mathrm{e}^{\mathrm{i}py/\hbar} \tag{2.70}$$

or in the momentum representation by

$$W(q, p) = \frac{1}{2\pi\hbar} \int \mathrm{d}z \langle p - z/2|\hat{\rho}|p + z/2\rangle \mathrm{e}^{-\mathrm{i}qz/\hbar}. \tag{2.71}$$

The Wigner representation of an operator $\hat{A}$ is then

$$A_{\mathrm{W}}(q, p) = \int_{-\infty}^{\infty} \mathrm{d}y \langle q - y/2|\hat{A}|q + y/2\rangle \mathrm{e}^{\mathrm{i}py/\hbar} \tag{2.72}$$

or can be evaluated analogously in momentum eigenstates. Wigner functions contain all the information present in the original density matrix, and in some ways resemble classical distribution functions, e.g.

$$\int_{-\infty}^{\infty} \mathrm{d}p \ W(q, p) = \langle x|\hat{\rho}|x\rangle, \tag{2.73}$$

$$\int_{-\infty}^{\infty} \mathrm{d}p \int_{-\infty}^{\infty} \mathrm{d}q \ W(q, p) = 1 \tag{2.74}$$

or

$$\int_{-\infty}^{\infty} \mathrm{d}p \int_{-\infty}^{\infty} \mathrm{d}q \; A_{\mathrm{W}}(q,p) W(q,p) = \langle \hat{A} \rangle = \mathrm{Tr}[\hat{A}\hat{\rho}]. \tag{2.75}$$

However, the Wigner function is not an actual classical distribution function for a quantum system — that would violate the Heisenberg uncertainty principle. If we took an arbitrary region of phase space and integrated over it to obtain the probability of finding the particle within a given range of positions and momenta, not only would we not get the correct value but we could also end up with negative probabilities.[37]

Nevertheless, Wigner functions form a bridge between the quantum and the classical description if appropriate limits are taken. The time evolution of the Wigner function can be derived by taking the Wigner transform of the time-evolution equation for the density operator $\partial\hat{\rho}/\partial t = (\mathrm{i}/\hbar)(\hat{\rho}\hat{H} - \hat{H}\hat{\rho})$ to obtain[23]

$$\frac{\partial W(q,p)}{\partial t} = -\hat{\mathcal{L}}_W W(q,p), \tag{2.76}$$

where the Wigner transformed Liouvillian is

$$\hat{\mathcal{L}}_W = \frac{p}{m}\frac{\partial}{\partial x} - \sum_{\ell=1,\mathrm{odd}}^{\infty} \left[\frac{1}{\ell!} \left(\frac{\mathrm{i}\hbar}{2} \right)^{\ell-1} \frac{\partial^\ell V(q)}{\partial q^\ell} \frac{\partial^\ell}{\partial p^\ell} \right]. \tag{2.77}$$

If we take the classical limit of $\hbar \to 0$, then we can truncate the infinite series at $\ell = 1$ to obtain[†]

$$\lim_{\hbar\to 0} \hat{\mathcal{L}}_W \approx \hat{\mathcal{L}}_{\mathrm{C}} = \frac{p}{m}\frac{\partial}{\partial x} - \frac{\partial V(q)}{\partial q}\frac{\partial}{\partial p}, \tag{2.78}$$

which is the classical Liouvillian for a phase space distribution. This truncation is exact if the potential is a harmonic oscillator.

[†]It may seem that the series itself is a sufficient justification for truncation in this limit, but one must also consider the derivatives of the potential and the Wigner function, which may yield additional powers of $\hbar$.[23] Nevertheless, this truncation is used in the widespread chemical dynamics method LSC-IVR.[38]

2.7.1 Wigner transform of HEOM

One can directly evaluate the Wigner transform of the terms in the equation for the time evolution of ADOs (eq. 2.61) to obtain the following relations

$$-\frac{\mathrm{i}}{\hbar}\hat{H}^{\times}\hat{\rho} \longrightarrow -\hat{\mathcal{L}}_{\mathrm{W}}W(q,p), \tag{2.79}$$

$$[\text{const}]\ \hat{\rho} \longrightarrow [\text{const}]\ W(q,p), \tag{2.80}$$

$$-\frac{\mathrm{i}}{\hbar}\hat{q}^{\times}\hat{\rho} \longrightarrow +\frac{\partial}{\partial p}W(q,p), \tag{2.81}$$

$$\hat{q}^{\circ}\hat{\rho} \longrightarrow 2qW(q,p), \tag{2.82}$$

which give rise to the phase space formulation of the hierarchical equations of motion

$$\frac{\partial W_{\boldsymbol{n}}}{\partial t} = -\left(\hat{\mathcal{L}}_{\mathrm{W}} + \sum_{k=0}^{\infty} n_k\gamma_k\right)W_{\boldsymbol{n}} + \sum_{k=0}^{\infty}\frac{\partial W_{\boldsymbol{n}_k^{\oplus}}}{\partial p} - \frac{\mathrm{i}}{\hbar}(\mathrm{i}n_0C_0^{\mathrm{I}})2qW_{\boldsymbol{n}_0^{\ominus}} + \sum_{k=0}^{\infty} n_kC_k^{\mathrm{R}}\frac{\partial W_{\boldsymbol{n}_k^{\ominus}}}{\partial p}, \tag{2.83}$$

which is an exact representation of the quantum HEOM in phase space.

2.7.2 Bopp operator derivation

Directly evaluating Wigner transforms can be cumbersome and there is an alternative way of obtaining Wigner transformed operators. Assuming that an operator $A_{\mathrm{s}}(\hat{q},\hat{p})$ has been symmetrised (as described in reference [35]) its action on a density operator can simply be rewritten using Bopp operators as[35,36]

$$A_{\mathrm{s}}(\hat{q},\hat{p})\hat{\rho} \longrightarrow A_{\mathrm{s}}\left(q - \frac{\hbar}{2\mathrm{i}}\frac{\partial}{\partial p}, p + \frac{\hbar}{2\mathrm{i}}\frac{\partial}{\partial q}\right)W(q,p), \tag{2.84}$$

and similarly, if the ordering of the operators is reversed,

$$\hat{\rho}A_{\mathrm{s}}(\hat{q},\hat{p}) \longrightarrow A_{\mathrm{s}}\left(q + \frac{\hbar}{2\mathrm{i}}\frac{\partial}{\partial p}, p - \frac{\hbar}{2\mathrm{i}}\frac{\partial}{\partial q}\right)W(q,p). \tag{2.85}$$

Furthermore, this can be applied to products of operators as well, giving

$$A_{\mathrm{s}}(\hat{q},\hat{p})B_{\mathrm{s}}(\hat{q},\hat{p})\hat{\rho} \longrightarrow A_{\mathrm{s}}\left(q - \frac{\hbar}{2\mathrm{i}}\frac{\partial}{\partial p}, p + \frac{\hbar}{2\mathrm{i}}\frac{\partial}{\partial q}\right)B_{\mathrm{s}}\left(q - \frac{\hbar}{2\mathrm{i}}\frac{\partial}{\partial p}, p + \frac{\hbar}{2\mathrm{i}}\frac{\partial}{\partial q}\right)W(q,p) \tag{2.86}$$

If our operators are symmetric (like $\hat{q}$ and $\hat{p}$) or easy to symmetrise, Bopp operators offer an easier way of expressing the Wigner operators. However, for more complicated operators, symmetrising the operator may be as complicated as evaluating the Wigner transform directly.[35]

2.7.3 Classical HEOM

Upon taking the limit $\hbar \to 0$ for the phase space representation of HEOM (eq. 2.83), we obtain fully classical hierarchical equations of motion

$$\frac{\partial W_n}{\partial t} = -\left(\hat{\mathcal{L}}_{\mathrm{C}} + n\gamma\right) W_n + \frac{\partial W_{n+1}}{\partial p} + \frac{n\eta\gamma}{\beta}\left(\frac{\partial}{\partial p} - \beta\gamma q\right) W_{n-1}. \tag{2.87}$$

All the Matsubara terms from the bath-coordinate time autocorrelation function α (eq. 2.51) have disappeared, the Liouvillian is now classical (as shown before in eq. 2.78) and the small angle approximation was used to simplify the term involving the cotangent. This leads to a one-dimensional hierarchy, just like in high temperature quantum HEOM in section 2.6.2.

Chapter 3

Computational implementation of quantum and classical hierarchical equations of motion

Quantum hierarchical equations of motion (HEOM) were implemented and tested in their reduced high-temperature form, where Matsubara terms from the bath time autocorrelation function are omitted. This is presented in section 3.1. Classical HEOM in position-momentum phase space are studied in section 3.2. Following the low-temperature breakdown of the previous implementation of quantum HEOM, their full form including the Matsubara terms was investigated in section 3.3. Two anharmonic potentials were studied using the implemented methods: a Morse oscillator in section 3.3.2 and a fitted OH potential of a hydrated oxonium ion in section 3.3.3.

3.1 High-temperature quantum HEOM

Taking the work of Tanimura and Wolynes as inspiration,[18] the high-temperature quantum HEOM described by eq. 2.65 were implemented.

The density matrix was represented in the basis of position eigenvectors $q_i \equiv \delta(q - q_i)$. The position operator and the potential energy operator are diagonal in this representation, giving

$$\begin{aligned}\frac{\partial \rho_n(q_i, q_j)}{\partial t} = &- \left(\frac{\mathrm{i}}{\hbar}\hat{\mathcal{L}} + n\gamma\right)\rho_n(q_i, q_j) - \frac{\mathrm{i}}{\hbar}(q_i - q_j)\rho_{n+1}(q_i, q_j) \\ &- \frac{n_0\eta\gamma^2}{2}(q_i + q_j)\rho_{n-1}(q_i, q_j) \\ &- \frac{\mathrm{i}}{\hbar}\frac{n\hbar\eta\gamma^2}{2}\cot\left(\frac{\beta\hbar\gamma}{2}\right)(q_i - q_j)\rho_{n-1}(q_i, q_j).\end{aligned} \tag{3.1}$$

To express the Hamiltonian in this basis, a discrete variable representation (DVR) matrix for the second derivative (the momentum operator) was used to obtain[39]

$$H_{\mathrm{S}}(q_i, q_j) = \begin{cases} V(q_i) + \frac{\hbar^2\pi^2}{6m(\Delta q)^2} & \text{for } i = j, \\ \frac{\hbar^2}{m(\Delta q)^2(i-j)^2}(-1)^{i-j} & \text{otherwise,} \end{cases} \tag{3.2}$$

where $\Delta q \equiv q_{i+1} - q_i$ is the position grid spacing. The equations of motion were then integrated in time using the fourth-order Runge-Kutta method.[40,41]

The general behaviour was investigated in a shifting harmonic potential as described in section 3.1.1 and position time autocorrelation functions were calculated (TCFs) in section 3.1.2. As expected, these simulations deteriorated with decreasing temperature, when the truncation of the bath-coordinate time autocorrelation function α (eq. 2.51) gives an increasingly large error.

3.1.1 Shifting potential

To test this set-up, we implemented the system presented in Tanimura's original paper,[18] which is a harmonic oscillator with a variable linear term given by

$$V_{\mathrm{S}}(q) = \frac{m\Omega^2}{2}q^2 - Fq, \tag{3.3}$$

where

$$F = \begin{cases} 0 & \text{for } t < 0 \\ 6 & \text{for } t \geq 0 \end{cases}, \tag{3.4}$$

$\Omega = 2$ and $m = 1$, all in atomic units. The initial state in the simulation was the Boltzmann distribution for the isolated system, which is given by

$$\rho_0(q_i, q_j) = \sqrt{\frac{m\Omega}{2\pi\hbar \sinh(\beta\hbar\Omega)}} \times \exp\left[-\frac{m\Omega}{2\pi\hbar \sinh(\beta\hbar\Omega)}\left[(q_i^2 + q_j^2)\cosh(\beta\hbar\Omega) - 2q_i q_j\right]\right] \quad (3.5)$$

with all ADOs set to zero (i.e. the factorised initial condition of eq. 2.20).

The system was allowed to equilibrate and then the potential was shifted, which resulted in damped oscillations. This behaviour is shown in fig. 3.1. The rate of the damping is affected both by the bath strength η and by the cutoff frequency γ, which is illustrated in figure 3.2. Both of these trends follow the expected behaviour. Increasing the strength of the bath coupling leads to higher damping and so does increasing the cutoff frequency.

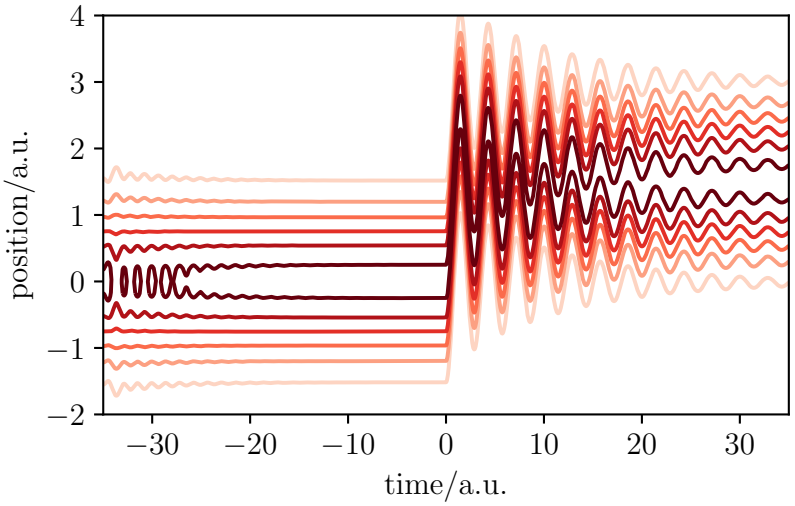

Figure 3.1: A contour plot of a wavepacket being equilibrated with a bath in a harmonic potential centered at $q = 0$. At $t = 0$ the potential is shifted by an addition of a linear term, which creates a new minimum at $q = 3/2$ a.u. This is a reproduction of a similar calculation from Tanimura, Wolynes, *Phys. Rev. A*, 1991, **43**, 4131–4142.

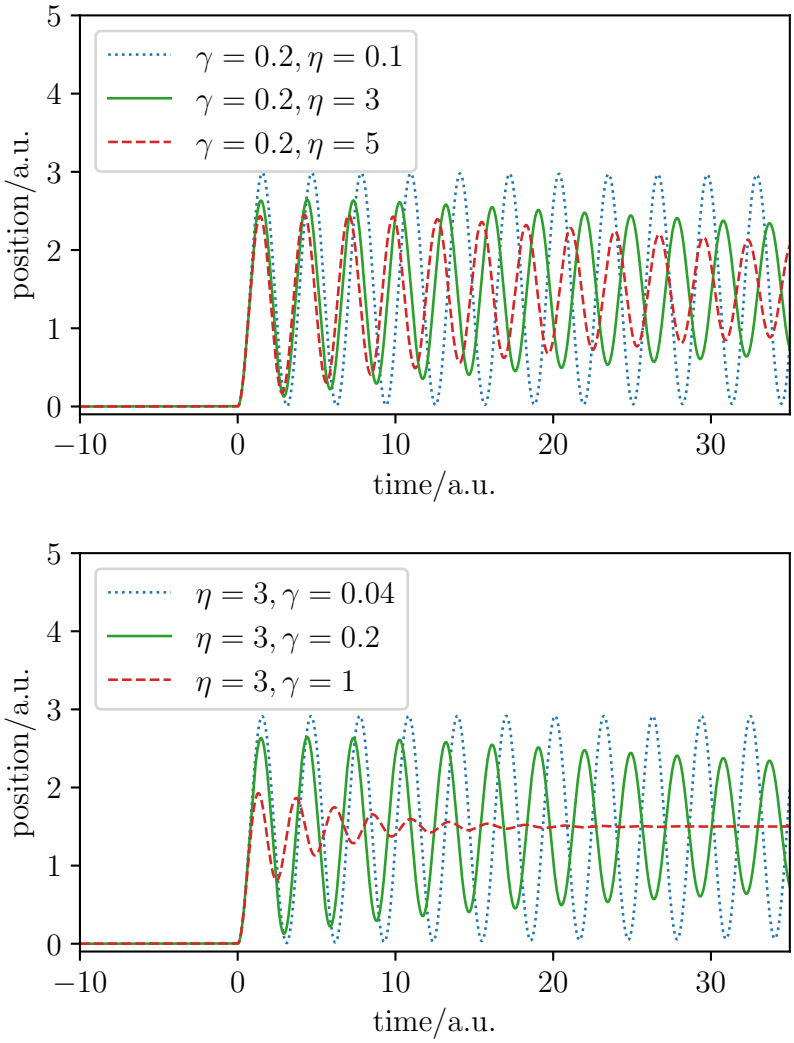

Figure 3.2: Displacement of the wavepacket centre (average) for a set-up described in fig. 3.1 as a function of the bath strength η and the bath cutoff frequency γ.

3.1.2 Harmonic potential TCFs

Dynamical properties of quantum systems are often described using time correlation functions (TCFs). These can then be used to predict vibrational spectra, diffusion coefficients, reaction rates and many other experimental observables.[12,24] We have chosen the position time autocorrelation function as a good means of probing the system, because it is closely related to the infra-red vibrational spectrum. The TCF is defined as

$$C_{qq}(t) = \langle \hat{q}(\tau)\hat{q}(\tau+t)\rangle = \langle \hat{q}(0)\hat{q}(t)\rangle = \\ = \mathrm{Tr}\left[\hat{\rho}\hat{q}(0)\hat{q}(t)\right] = \mathrm{Tr}\left[\hat{\rho}\hat{q}\mathrm{e}^{+\mathrm{i}\hat{H}t/\hbar}\hat{q}\mathrm{e}^{-\mathrm{i}\hat{H}t/\hbar}\right], \quad (3.6)$$

where we have used the fact that for an equilibrium state TCFs are independent of the time origin.[†] The last expression can be evaluated by propagating the density matrix $\hat{\rho}\hat{q}$ in time using the HEOM and then acting on it by $\hat{q}$ and summing the trace for each sampled time.

A useful way of presenting TCFs is by taking their Fourier transform, which is also called the power spectrum, and is given by

$$G_{qq}(\omega) = \int_{-\infty}^{\infty} \mathrm{d}t\ \mathrm{e}^{\mathrm{i}\omega t} C_{qq}(t). \quad (3.7)$$

Assuming that the dipole moment is proportional to the displacement of our system, and employing Fermi's golden rule, the power spectrum can be related to the vibrational absorption spectrum as[24]

$$I(\omega) \propto \omega(1-\mathrm{e}^{-\beta\hbar\omega})G_{qq}(\omega), \quad (3.8)$$

where the frequency-independent constant of proportionality depends the on physical parameters of the measurement. All spectra in this work are presented in arbitrary units.

In the TCF of the harmonic oscillator system described in the previous section we can clearly see the damping effect of the "random force" of the bath, which leads to a loss of coherence and decorrelation as shown in figure 3.3. Increasing the cutoff frequency of the bath γ leads to shorter decorrelation times. This can also be observed in the spectrum as broadening and shifting of the peak. It should be noted that the blue shift is due to the renormalisation potential of eq. 2.10, rather than the dynamics of the bath.

[†]This is due to the commutation of the time evolution and Boltzmann density operator for time independent Hamiltonians.

When the temperature is sufficiently low ($\beta\hbar\Omega \gg 1$), we observe non-physical "beats" which are an artefact of the truncation of the bath-coordinate time autocorrelation function α (eq. 2.51). At very low temperatures the TCF simply diverges without ever being damped to zero. In addition, during equilibration at low temperatures, the wave packets have a tendency to dissolve, grow rapidly, change shape or drift, all of which make simulations less stable as well as non-physical. This is illustrated in figure 3.4 where the TCF becomes well behaved only for very short times with increasing β. Similar behaviour was observed for anharmonic potentials in sections 3.3.2 and 3.3.3.

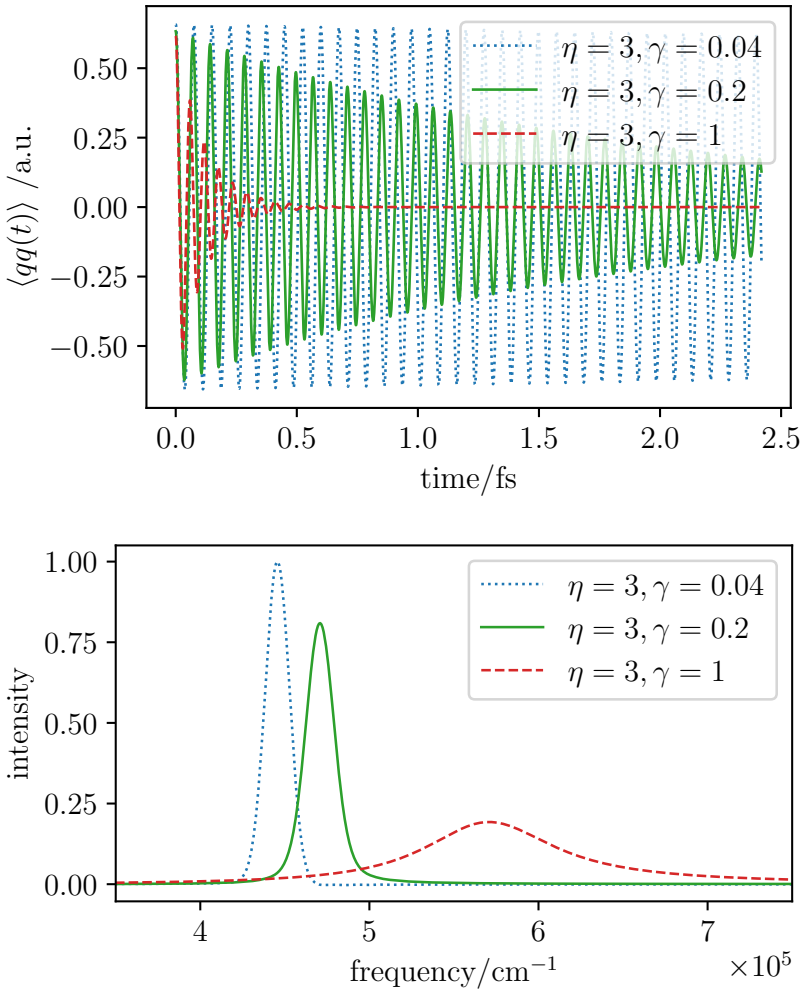

Figure 3.3: Position time-autocorrelation function and its spectrum for the harmonic oscillator model system from Tanimura, Wolynes, *Phys. Rev. A*, 1991, **43**, 4131–4142, calculated using high temperature HEOM with truncated Matsubara terms in the bath time autocorrelation function as a function of the bath cutoff frequency γ at $\beta = 0.4$ a.u.

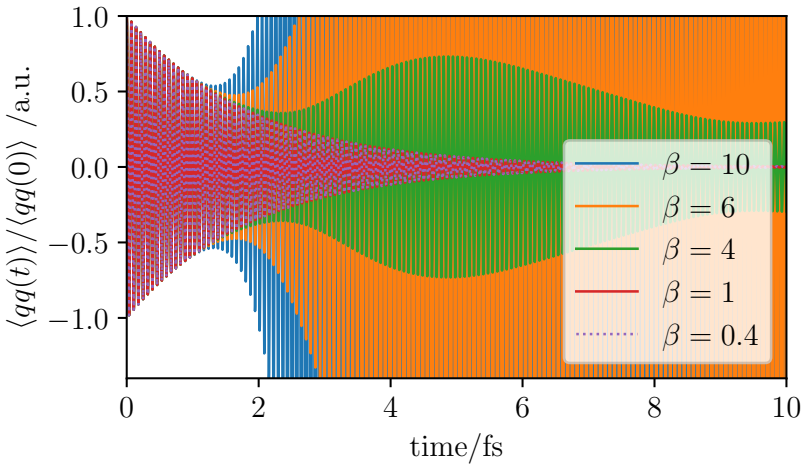

Figure 3.4: Normalised position time autocorrelation functions of the harmonic oscillator from fig. 3.3 showing artificial beats when temperature enters the quantum regime ($\beta\hbar\Omega \gg 1$). These artefacts are a consequence of the truncation of the Matsubara terms in the bath time autocorrelation function.

3.2 Classical HEOM

Similarly to quantum HEOM in section 3.1, classical HEOM propagation given by eq. 2.87 was implemented. Wigner functions were represented in a discretised position-momentum phase space to give

$$\frac{\partial W_n(q_i,p_j)}{\partial t} = -\left(\hat{\mathcal{L}}_{\mathrm{C}} + n\gamma\right) W_n(q_i,p_j) + \frac{\partial W_{n+1}(q_i,p_j)}{\partial p} + \frac{n\eta\gamma}{\beta}\left(\frac{\partial}{\partial p} - \beta\gamma q\right) W_{n-1}(q_i,p_j). \quad (3.9)$$

To construct the first derivative matrices, an appropriate discrete variable representation (DVR) matrix was derived analogously to the second derivative matrix presented in reference [39] to give

$$D_{ij} = \frac{\pi}{(N+1)L} \times \begin{cases} Y\left(\frac{(i+j)\pi}{N+1}\right) & \text{for } i = j, \\ Y\left(\frac{(i+j)\pi}{N+1}\right) + Y\left(\frac{(i-j)\pi}{N+1}\right) & \text{otherwise,} \end{cases} \quad (3.10)$$

with

$$Y(x) = \frac{+N\sin\left[(N+1)x\right] - (N+1)\sin(Nx)}{2(1-\cos x)}, \quad (3.11)$$

where N is the number of grid points and $L \equiv q_N - q_0$ is the span of the grid.

Similar tests to those described for quantum HEOM in section 3.1 were carried out. The response to the shifting harmonic oscillator is presented in section 3.2.1 and calculation of TCFs in section 3.2.2.

3.2.1 Shifting potential

Using the same set-up as described in section 3.1.1, a wavepacket was propagated in a shifting potential. Similar studies to those presented for quantum HEOM were carried out and are shown in figures 3.5 and 3.6 side by side with the quantum calculations. The trends are the same as before. Increasing bath strength η and increasing cutoff frequency γ both increase damping. However, the dynamics is different and the classical wave packet oscillates at a higher frequency compared to its quantum counterpart. Upon decreasing the temperature, classical HEOM begins to exhibit a similar divergent behaviour to that of fig. 3.4 which leads to poor stability of the calculations.

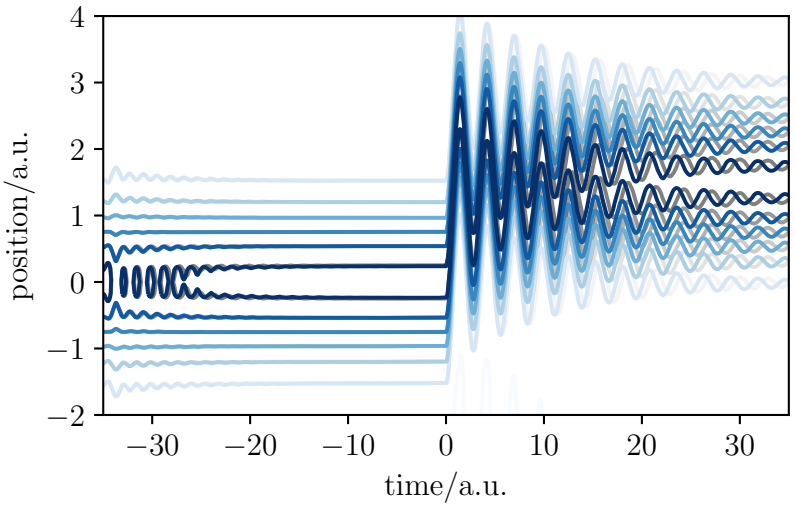

Figure 3.5: A contour plot of the same shifting potential set-up presented in fig. 3.1 with classical HEOM in blue and the quantum analogue in grey.

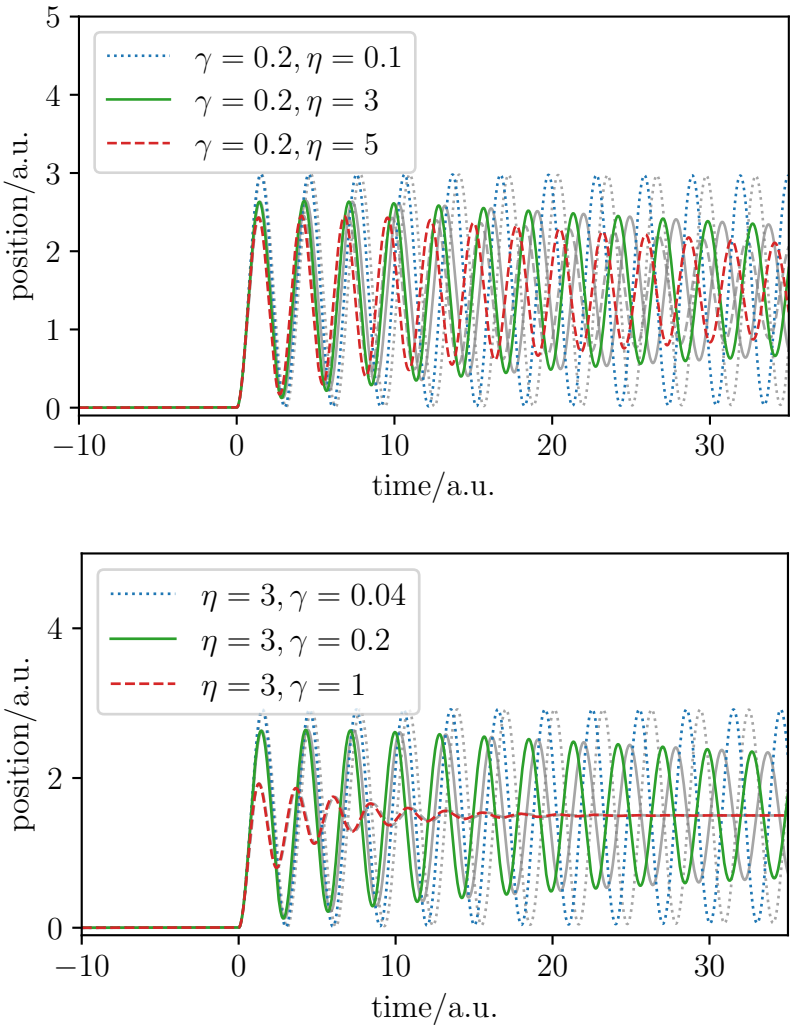

Figure 3.6: Displacement of the wavepacket centre (average) for a set-up identical to that of fig. 3.2 as a function of the bath strength η and the bath cutoff frequency γ with classical HEOM in colour and the quantum analogues in grey.

3.2.2 Harmonic potential TCFs

As shown in figure 3.7, the trend of decreasing decorrelation time with increasing bath strength and cutoff frequency is qualitatively the same as for quantum HEOM. Classical HEOM, however, shows a blue shift relative to the quantum result.

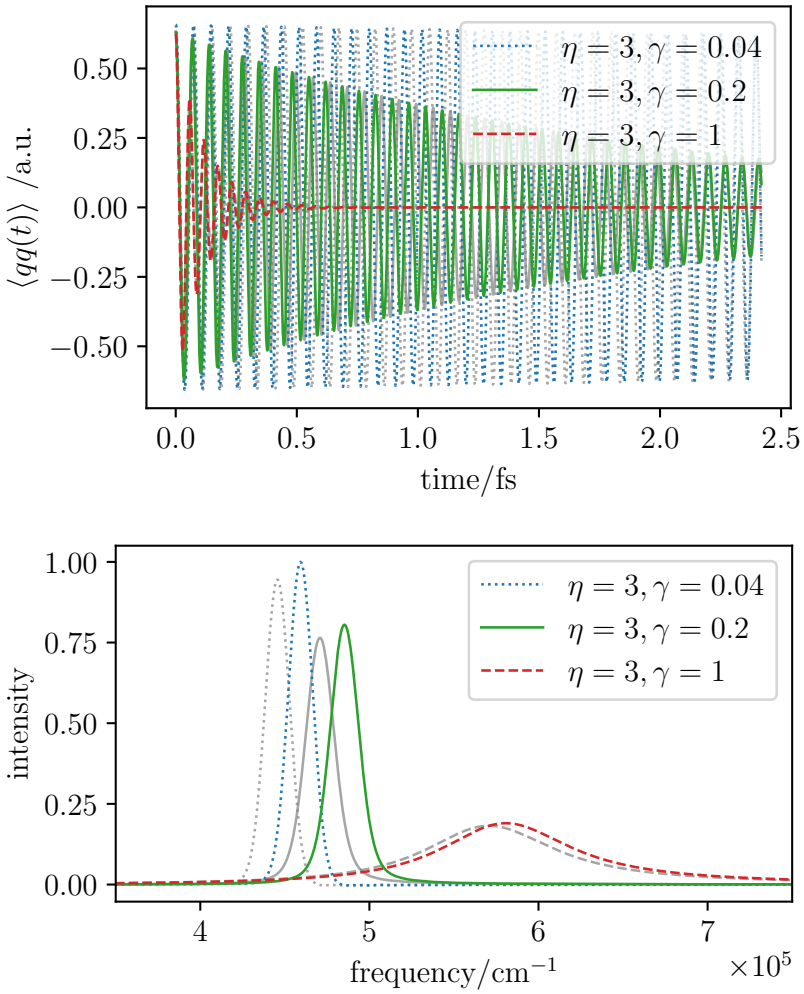

Figure 3.7: Position time autocorrelation functions with changing bath cutoff frequency γ and their spectra for a set-up identical to fig. 3.3 with classical HEOM in colour and the quantum analogues in grey.

3.3 Low-temperature quantum HEOM

As shown in section 3.1, at low temperatures the Matsubara terms in the bath become necessary for a correct physical description. Therefore, one must use the full quantum HEOM given by equation 2.61. This requires a new computational treatment since ADOs are now spread across a $K+1$ dimensional space. In addition, it is not computationally feasible to represent all ADOs up to a hard cutoff L (i.e. with tiers $n \leq L$) because their number grows combinatorially.[†]

This has been solved by implementing the ADO hierarchy using a Python dictionary in combination with the pruning mechanism described in section 2.6.3. Even then, the number of ADOs is quite large and their interaction more complex, which leads to higher computational requirements. For simulations with static potentials at low temperatures, however, one can transform the HEOM into the space of Hamiltonian eigenvectors (of the system Hamiltonian $\hat{H}_{\mathrm{S}}$). These were obtained by direct diagonalisation of the DVR Hamiltonian (eq. 3.2). This representation leads to much smaller matrices than in the position eigenstate representation and makes calculations more tractable. To improve the rate of equilibration, the initial state for the anharmonic potentials was taken to be the Boltzmann distribution of the DVR energy levels, as opposed to the analytical distribution for the harmonic oscillator (eq. 3.5). The exact initial state is, however, irrelevant, assuming that the system is properly equilibrated before the measurement.

In the next section we have shown that the Matsubara terms correct the previous non-physical beating in the TCFs. To test our model on anharmonic potentials we chose two systems from the literature. A Morse oscillator system investigated by Sakurai and Tanimura[20] is presented in section 3.3.2 and a quartic fit of a hydrated oxonium OH bond potential by Yu and Bowman[42] in section 3.3.3.

[†]One can easily show that $N_{\mathrm{ADOs}}(L,K) = \sum_{n=0}^{L} \binom{n+K}{n}$. (This is an example of the so called "stars and bars" combinatorics problem.)

3.3.1 Harmonic potential TCFs

The importance of Matsubara terms in the bath autocorrelation function α (eq. 2.51) was demonstrated in figure 3.4, where lowering the temperature lead to beating or even divergence of the TCF. As figure 3.8 demonstrates, at $\beta = 10$ a.u., which is deep in the "quantum regime" ($\beta\hbar\Omega = 20 \gg 1$), two Matsubara terms are already qualitatively correct, with $K = 3$ yielding the converged result. The number of Matsubara modes required increases with decreasing temperature as expected, since more terms in the exponential series of α will contribute.

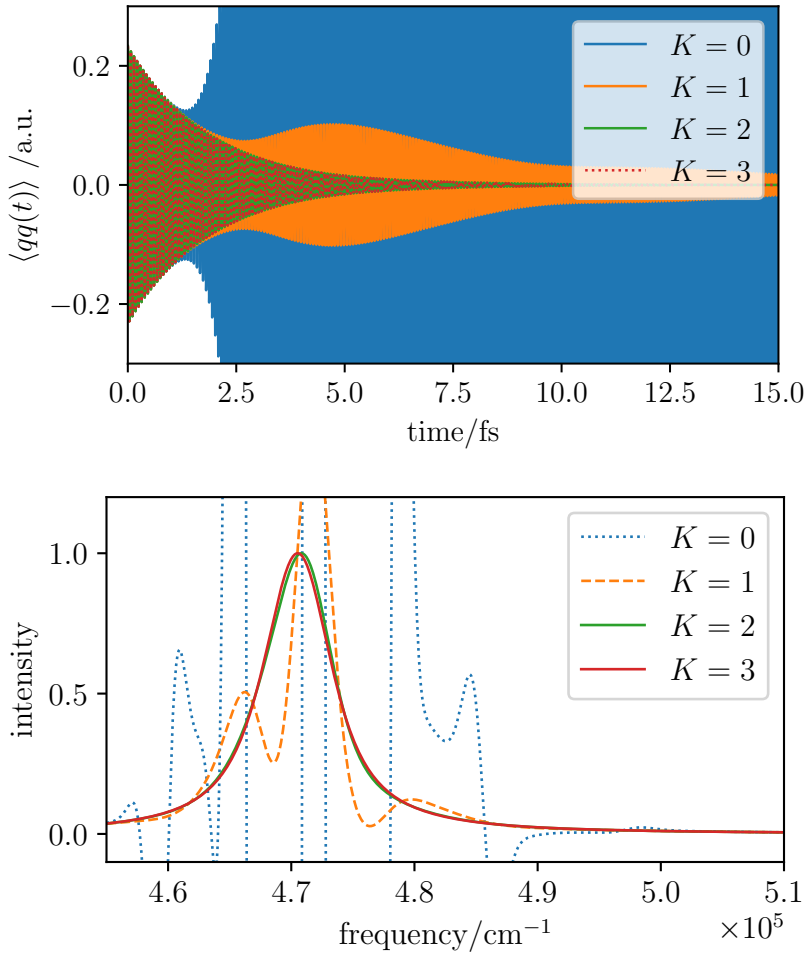

Figure 3.8: Low temperature correction to a TCF from figure 3.4 at $\beta = 10$ a.u. and its spectrum. It can be seen that at this temperature inclusion of two Matsubara terms already leads to an almost converged result and three are sufficient. Decreasing temperature leads to an increase in the number of required Matsubara terms in the bath autocorrelation function.

3.3.2 Morse potential TCFs

Tanimura and Sakurai have studied HEOM spectra for the Morse potential,[20] which is defined as

$$V_{\text{Morse}}(q) = D_{\text{e}} \left(1 - \mathrm{e}^{-\alpha q}\right)^2, \tag{3.12}$$

where D_{e} is the depth of the potential well and α is the stiffness coefficient. They chose the values $\Omega_{10} = 1600$ cm^{-1} and $\Delta_{\text{anh}} = 16$ cm^{-1} which are related to potential parameters as $\Delta_{\text{anh}} = \hbar\alpha^2/m$ and $\Omega_{\text{c}} = \sqrt{2D_{\text{e}}\alpha^2/m}$ with $\Omega_{10} = \Omega_{\text{c}} - \Delta_{\text{anh}}$. The authors relate these values to the Amide-I mode in peptides.

Calculations were carried out at the temperature of 300 K at which quantum effects are pronounced, with a bath strength $\eta = 0.05\Omega_{10}$, and with varying bath cutoff frequency $\gamma = 0.02\Omega_{10}$, $0.1\Omega_{10}$ and $0.5\Omega_{10}$. Sakurai and Tanimura's results are compared with our results in figure 3.9. The positions and shapes of peaks in our quantum HEOM spectra follow the published results closely, including a minor feature of the 1–2 transition at $\sim$1585 cm^{-1}. Despite our calculations being converged with respect to all parameters, the observed magnitude of this transition for the $\gamma = 0.02\Omega_{10}$ case was smaller than the reported value. The origin of this discrepancy is currently unknown.

As opposed to Sakurai's calculations which used a rigid cutoff in L with an anchor equation, in our simulation we settled with scaling and pruning due to Shi as described in section 2.6.3. This allows the number of ADOs to dynamically change during the simulation. Results have been converged both with respect to the number of Matsubara terms K and the pruning cutoff (equivalent to converging w.r.t. L). It was found that inclusion of the low temperature correction due to Tanimura (eq. 2.66) improves the K-convergence greatly. This effect is particularly pronounced during equilibration, where the drift of the wave packets described in section 3.1.2 shows relatively slow convergence without the correction.

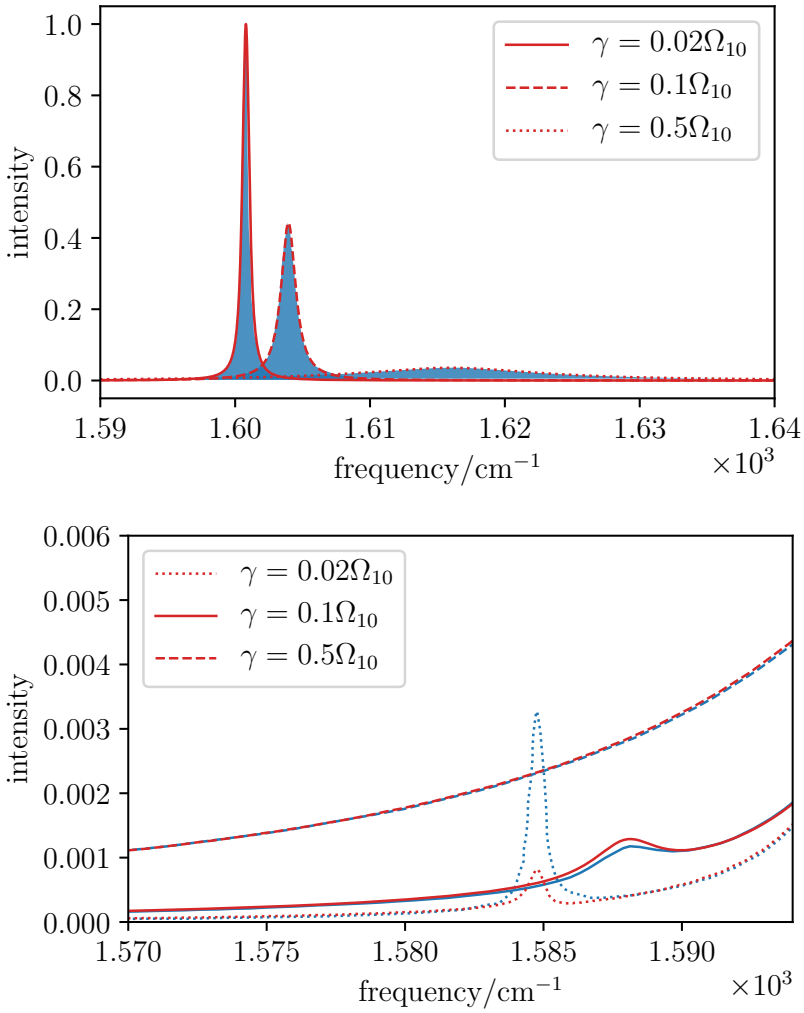

Figure 3.9: Morse oscillator quantum HEOM spectra at 300 K with varying bath cutoff frequency γ and a magnification of the 1–2 transition. The shaded areas in the first graph and the blue lines in the second are the results extracted from Sakurai, Tanimura, *J. Phys. Chem. A*, 2011, **115**, 4009-4022.

3.3.3 Anharmonic OH model TCFs

Yu and Bowman have recently published their calculation of water cluster vibrational spectra.[42] Most commonly used quantum dynamics methods, including thermostatted ring-polymer molecular dynamics (TRPMD), perform poorly in these strongly anharmonic potentials.[42]

Raz Benson investigated this behaviour, by fitting the $H_7O_3^+$ OH potential used by Bowman with a quartic polynomial, and calculating its white-noise TRPMD TCFs. The form of the potential is

$$V_{\mathrm{S}}[\mathrm{a.u.}] = 0.1297q^2 + c(0.1657q^4 - 0.2467q^3), \tag{3.13}$$

where c is the anharmonicity coefficient, which for $c = 1$ gives a quartic fit to the original potential. The temperature was set to 100 K and the effective mass used is $m = 1837.3622$ a.u.

Benson's preliminary results show a large blue shift relative to exact quantum results as shown in figure 3.10.[†] Because we are particularly interested in the blue shift, we decided to set $a_{\mathrm{ren}} = 0$ in our HEOM calculations. Otherwise, the renormalisation potential in eq. 2.10 would lead to a blue shift simply by increasing the effective spring constant of the potential. In other terms, we used the convention, in which the renormalisation potential is taken to be a part of the system potential. Other parameters were set to $\eta = 5$ and $\gamma = 0.1\Omega_{\mathrm{h}}$, where Ω_{h} is the frequency for the harmonic case ($c = 0$). The bath strength was chosen such that damping is substantial on the time scale of ∼500 fs, which is a typical decorrelation time for liquid water.[43]

One hypothesis on the possible sources of the TRPMD blue shift relative to DVR is the lack of quantum coherence in PIMD-based methods. HEOM not coupled to the bath ($\eta = 0$) gives results identical to DVR and one of the effects of coupling a system to a bath is loss of coherence. If this were a major contributor to the blue shift, we would expect to see HEOM shifted to higher frequencies relative to DVR. However, it was observed that under the previously described set-up, inclusion of a bath results in a small red shift relative to DVR as shown in fig. 3.11. It is not clear at this stage which effects are simply mechanical and which might be due to loss of coherence, but the collected data does not support the presented hypothesis.

[†]Exact quantum results were obtained using discrete variable representation (DVR)[39] Hamiltonian and expansion of eq. 3.6 in energy eigenstates.

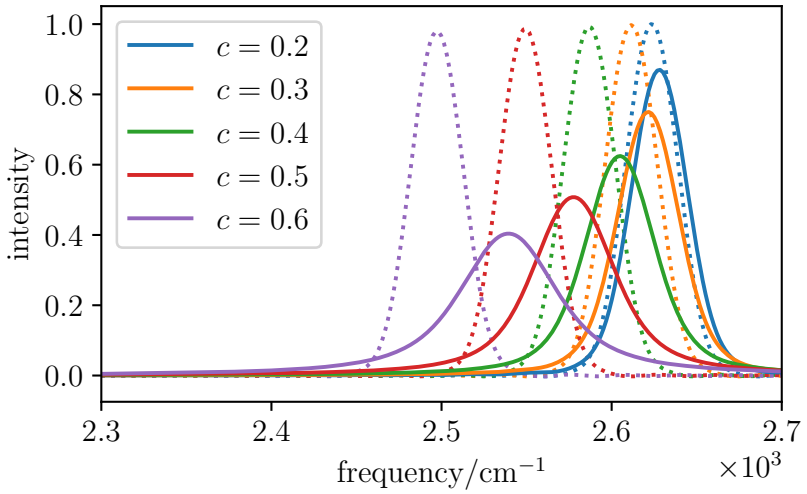

Figure 3.10: Benson's white-noise TRPMD spectra for a quartic fit to a hydrated oxonium ion OH potential compared with exact quantum DVR calculations. The coefficient c defines the level of anharmonicity of the potential with $c = 0$ being completely harmonic. TRPMD data are shown in full lines and DVR in dotted lines.

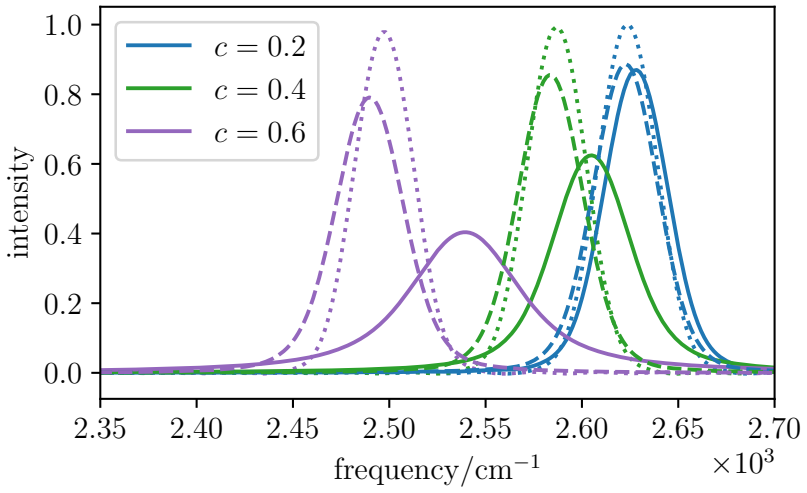

Figure 3.11: Comparison of HEOM spectra for non-renormalised potential with DVR and TRPMD data from figure 3.10. TRPMD is shown in full lines, DVR in dotted lines and HEOM in dashed lines. Data for $c = 0.3$ and 0.5 were omitted for clarity, but they show the same trend.

Chapter 4

Conclusions and further work

Hierarchical equations of motion (HEOM) are an exact description of the propagation of a quantum system coupled to a bath due to Tanimura. They are a versatile tool for computing dissipative quantum dynamics.[14,15,18,19]

In this work, a computer program capable of a range of HEOM simulations was developed. Firstly, a reduced version of HEOM was implemented, omitting the Matsubara frequency terms in the bath time autocorrelation function. Its behaviour was investigated under a range of conditions, including a breakdown for low temperatures. At such conditions, the position time autocorrelation functions were accurate only for very short times, but showing non-physical beats at longer times. In addition, the stability of the wave packets during equilibration was impaired, leading to artificial drifting or changes in shapes.

Taking a Wigner transform of the quantum HEOM followed by a high temperature limit leads to fully classical HEOM.[18] These were implemented using discretised position-momentum phase space representations of Wigner functions and a DVR-based first derivative matrices. Results obtained from these simulations were compared to the quantum results.

To correct for the breakdown of the reduced quantum HEOM, a full version containing the Matsubara terms of the bath correlation function[32] was implemented. It was shown how inclusion of these terms leads to a reduction and complete removal of the beats in the position time autocorrelation functions as well as to the mitigation of the instabilities during equilibration.

To test our implementation of HEOM, we have set out to reproduce Morse oscillator spectra at different bath cut-off frequencies which were originally presented by Sakurai and Tanimura.[20] Our calculations matched the published results closely.

Leading up to further work, we began an investigation of a hydrated oxonium ion OH bond potential from an article by Yu and Bowman.[42] They have shown that this potential is poorly tackled by most currently used quan-

tum dynamics methods. Raz Benson calculated white-noise thermostatted ring-polymer molecular dynamics (TRPMD) time correlation functions for a quartic fit to this potential with varying degrees of anharmonicity. TRPMD showed an increasingly large blue shift with increasing anharmonicity. This is a well known shortcoming of all path integral based quantum dynamics methods. One possible hypothesis was that the blue shift might be simply due to the omission of quantum coherence in this family of methods. In such case one would expect that HEOM, which describe coupling to a bath and consequent decoherence exactly, should reproduce at least some of the blue shift. Our calculations have shown that this is not the case. HEOM leads to a blue shift if the renormalisation potential is included, which, however, is a mechanical consequence of the set-up. If the renormalisation potential is set to zero, then a small red shift is observed instead. The origin of this shift could be purely mechanical or related to the coherence but in the light of this observation it seems unlikely that quantum coherence would be an major factor in the blue shift of TRPMD. This result is yet to be compared to related methods like centroid molecular dynamics (CMD)[4,5] and coloured noise TRPMD (TRPMD+GLE).[44]

In the following work, we would like to implement TRPMD with an explicit bath. This would give us access to both exact quantum results for a dissipative system, where quantum coherence can be quenched, as well as to an entirely equivalent system-bath ring-polymer set-up. Such a comparison has never been done and could bring new insight into the approximations inherent to ring-polymer methods as well as the role of quantum coherence in condensed phase dynamics.

A slightly more distant goal, which follows from our preliminary classical HEOM investigations, is implementing Matsubara dynamics with an explicit bath. Unlike in RPMD, which has been shown to work with an explicit set of harmonic oscillators,[45] in Matsubara dynamics it is impractical to do the same due to a severe phase problem.[8] Therefore, we seek an alternative route by implementing a bath for Matsubara dynamics using HEOM. Given that Matsubara dynamics is the least approximative of all ring-polymer based methods, such a description would help us to push the understanding of condensed phased quantum dynamics even further.

Bibliography

(1) M. Tuckerman, *Statistical Mechanics: Theory and Molecular Simulation*, Oxford University Press, 2010.

(2) T. E. Markland and M. Ceriotti, *Nat. Rev. Chem.*, 2018, **2**, 0109.

(3) R. Feynman and A. R. Hibbs, *Quantum Mechanics and Path Integrals*, Dover Publications, Inc., Mineola, New York, Emended, 2010.

(4) J. Cao and G. A. Voth, *J. Chem. Phys.*, 1994, **101**, 6168.

(5) S. Jang and G. A. Voth, *J. Chem. Phys.*, 1999, **111**, 2371.

(6) I. R. Craig and D. E. Manolopoulos, *J. Chem. Phys.*, 2004, **121**, 3368.

(7) H. Wang, X. Sun and W. H. Miller, *J. Chem. Phys.*, 1998, **108**, 9726–9736.

(8) T. J. H. Hele, M. J. Willatt, A. Muolo and S. C. Althorpe, *J. Chem. Phys.*, 2015, **142**, 134103.

(9) T. J. H. Hele, M. J. Willatt, A. Muolo and S. C. Althorpe, *J. Chem. Phys.*, 2015, **142**, 191101.

(10) D. Frenkel and B. Smit, *Understanding molecular simulation: from algorithms to applications*, Academic Press, 2001.

(11) U. Weiss, *Quantum Dissipative Systems*, World Scientific, 2012.

(12) A. Nitzan, *Chemical Dynamics in Condensed Phases*, Oxford University Press, 2013.

(13) R. Kubo, *J. Math. Phys.*, 1963, **4**, 174–183.

(14) Y. Tanimura, *J. Phys. Soc. Japan*, Aug. 2006, **75**, 082001.

(15) Y. Tanimura, *Phys. Rev. A*, 1990, **41**, 6676–6687.

(16) Y. Tanimura and R. Kubo, *J. Phys. Soc. Japan*, 1989, **58**, 101–114.

(17) Y. Tanimura, T. Suzuki and R. Kubo, *J. Phys. Soc. Japan*, 1989, **58**, 1850–1859.

(18) Y. Tanimura and P. G. Wolynes, *Phys. Rev. A*, 1991, **43**, 4131–4142.

(19) Y. Tanimura and P. G. Wolynes, *J. Chem. Phys.*, 1992, **96**, 8485–8496.

(20) A. Sakurai and Y. Tanimura, *J. Phys. Chem. A*, 2011, **115**, 4009–4022.

(21) L. Chen and Q. Shi, *J. Chem. Phys.*, 2009, **130**, 134505.

(22) C. Kreisbeck, T. Kramer, M. Rodríguez and B. Hein, *J. Chem. Theory Comput.*, 2011, **7**, 2166–2174.

(23) L. E. Ballentine, *Quantum Mechanics: A Modern Development*, World Scientific, 1998.

(24) R. Zwanzig, *Nonequilibrium Statistical Mechanics*, Oxford University Press, 2001.

(25) J. J. Sakurai and J. Napolitano, *Modern Quantum Mechanics*, Cambridge University Press, 2017.

(26) A. Caldeira and A. Leggett, *Physica A*, 1983, **121**, 587–616.

(27) R. Feynman and F. Vernon, *Ann. Phys.*, 1963, **24**, 118–173.

(28) A. Caldeira and A. Leggett, *Ann. Phys.*, 1983, **149**, 374–456.

(29) H. Grabert, U. Weiss and P. Talkner, *Phys. B Condens. Matter*, 1984, **55**, 87–94.

(30) A. Ishizaki and Y. Tanimura, *J. Phys. Soc. Japan*, 2005, **74**, 3131–3134.

(31) R.-X. Xu and Y. Yan, *Phys. Rev. E*, Mar. 2007, **75**, 031107.

(32) Q. Shi, L. Chen, G. Nan, R.-X. Xu and Y. Yan, *J. Chem. Phys.*, 2009, **130**, 084105.

(33) A. Ishizaki and Y. Tanimura, *J. Chem. Phys.*, Aug. 2006, **125**, 084501.

(34) Y. Tanimura, *J. Chem. Phys.*, 2014, **141**, 044114.

(35) R. Kubo, *J. Phys. Soc. Japan*, 1964, **19**, 2127–2139.

(36) M. Hillery, R. F. O'Connell, M. O. Scully and E. P. Wigner, *Phys. Rep.*, 1984, **106**, 121–167.

(37) W. B. Case, *Am. J. Phys.*, Oct. 2008, **76**, 937–946.

(38) Q. Shi and E. Geva, *J. Chem. Phys.*, 2003, **118**, 8173–8184.

(39) D. T. Colbert and W. H. Miller, *J. Chem. Phys.*, 1992, **96**, 1982–1991.

(40) W. H. Press, S. A. Teukolsky, B. P. Flannery and W. T. Vetterling, *Numerical Recipes in FORTRAN 77: Volume 1*, Cambridge University Press, 1992.

(41) W. H. Press, W. T. Vetterling, M. Metcalf, S. A. Teukolsky and B. P. Flannery, *Numerical Recipes in Fortran 90: Volume 2*, Cambridge University Press, 1996.

(42) Q. Yu and J. M. Bowman, *J. Phys. Chem. A*, 2019, **123**, 1399–1409.

(43) S. Woutersen and H. J. Bakker, *Phys. Rev. Lett.*, 1999, **83**, 2077–2080.

(44) M. Rossi, V. Kapil and M. Ceriotti, *J. Chem. Phys.*, Mar. 2018, **148**, 102301.

(45) I. R. Craig and D. E. Manolopoulos, *J. Chem. Phys.*, 2005, **122**, 084106.